ZOONOTIC DISEASES

Multiomic profiling of cutaneous leishmaniasis infections reveals microbiota-driven mechanisms underlying disease severity

Camila Farias Amorim[1], Victoria M. Lovins[2], Tej Pratap Singh[1], Fernanda O. Novais[3], Jordan C. Harris[2], Alexsandro S. Lago[4], Lucas P. Carvalho[4,5], Edgar M. Carvalho[4,5], Daniel P. Beiting[1], Phillip Scott[1]*, Elizabeth A. Grice[2]*

Leishmania braziliensis is a parasitic infection that can result in inflammation and skin injury with highly variable and unpredictable clinical outcomes. Here, we investigated the potential impact of microbiota on infection-induced inflammatory responses and disease resolution by conducting an integrated analysis of the skin microbiome and host transcriptome on a cohort of 62 patients infected with *L. braziliensis*. We found that overall bacterial burden and microbiome configurations dominated with *Staphylococcus* spp. were associated with delayed healing and enhanced inflammatory responses, especially by IL-1 family members. Quantification of host and bacterial transcripts on human lesions revealed that high lesional *S. aureus* transcript abundance was associated with delayed healing and increased expression of IL-1β. This cytokine was critical for modulating disease outcomes in *L. braziliensis*–infected mice colonized with *S. aureus*, given that its neutralization reduced pathology and inflammation. These results highlight how the human microbiome can shape disease outcomes in cutaneous leishmaniasis and suggest pathways toward host-directed therapies to mitigate the inflammatory consequences.

INTRODUCTION

Cutaneous leishmaniasis is a zoonotic neglected tropical disease caused by protozoan parasites transmitted by sand fly bites. The clinical manifestation of leishmania infection is highly variable, ranging from single, self-resolving skin lesions to severe chronic ulcers, including disseminated and mucosal manifestations, all of which can be disfiguring (*1–4*). The parasite burden and the host immune response can influence where a patient falls on this clinical spectrum. Some of the most severe forms of the disease are characterized by chronic inflammation despite parasite control (*2*). Parasite-targeted drug treatment, such as pentavalent antimony (Sb^v), is associated with high rates of failure in some endemic areas, and no vaccine for the disease currently exists. Thus, identifying mechanisms that drive destructive immunopathologic responses could provide additional therapeutic targets to ameliorate the more severe forms of cutaneous leishmaniasis.

The skin microbiome contributes to homeostatic mechanisms that fortify the skin's barrier function (*5*). In contrast, a breach of the skin barrier, such as that caused by leishmania infection, can disturb the commensal microbiota and expose underlying tissues to invasion by microbes (*6*). Several studies suggest that the skin microbiome promotes increased disease in experimental models of cutaneous leishmaniasis (*7–9*). Germ-free mice infected with

Leishmania major develop smaller lesions than those observed in conventional mice, and colonization of germ-free mice with *Staphylococcus epidermidis* restores ulcer development in *L. major*–infected mice (*8*). In conventionally raised mice, colonization or coinfection with *Staphylococcus aureus*, *S. epidermidis*, or *Staphylococcus xylosus* promotes increased lesional pathology, accompanied by increased inflammation and higher expression of proinflammatory cytokines, such as interleukin-1β (IL-1β) and IL-17 in lesions, compared with infection with *L. major* alone (*7*, *9*, *10*). Although these experimental models suggest a pathological role for the microbiota, the relevance of these findings to the clinical course of human *Leishmania* infection and lesion resolution remains unclear.

To address this gap, we conducted an integrative multiomics meta-analysis in a cohort of patients with *Leishmania braziliensis*. We performed 16*S* ribosomal RNA (rRNA) amplicon sequencing (16*S*-seq) of lesional and contralateral skin swabs to profile the microbial communities longitudinally. In parallel, lesional biopsies were collected for RNA sequencing (RNA-seq) to profile the host transcriptome and quantify total bacterial burden. Bacterial burden was increased in lesions compared with intact, contralateral skin, and lesional burden correlated with proinflammatory host gene expression and delayed healing. Lesions were grouped into eight distinct clusters based on 16*S*-seq profiles, but most fell within a cluster defined by the high relative abundance of the genus *Staphylococcus*. We constructed a custom *S. aureus* pangenome using clinical isolates and quantified *S. aureus* reads detected in each lesional biopsy. High *S. aureus* read counts were associated with increased expression of cytolytic-encoding genes and IL-1–related gene transcription. We found delayed healing in patients with high *S. aureus* read counts. Last, to determine whether *S. aureus*–induced IL-1β contributes to increased disease, we neutralized IL-1β signaling in *L. braziliensis*–infected mice colonized with

[1]Department of Pathobiology, School of Veterinary Medicine, University of Pennsylvania, Philadelphia, PA 19104, USA. [2]Department of Dermatology, Perelman School of Medicine, University of Pennsylvania, Philadelphia, PA 19104, USA. [3]Department of Microbial Infection and Immunity, College of Medicine, Ohio State University, Columbus, OH 43210, USA. [4]Laboratório de Pesquisas Clínicas do Instituto de Pesquisas Gonçalo Muniz–Fiocruz, Salvador, Bahia 40296-710, Brazil. [5]Immunology Service, Professor Edgard Santos University Hospital Complex, Federal University of Bahia, Salvador, Bahia 40110-060, Brazil.
*Corresponding author. Email: egrice@pennmedicine.upenn.edu (E.A.G.); pscott@vet.upenn.edu (P.S.)

Farias Amorim *et al.*, *Sci. Transl. Med.* **15**, eadh1469 (2023)   18 October 2023

1 of 14

an *S. aureus* clinical isolate. Our findings confirmed that colonization with *S. aureus* promotes increased lesion size and pathology in an IL-1β–dependent manner. These findings demonstrate the impact of the skin microbiome on human leishmanial infections and highlight the potential of implementing microbiota-directed therapeutic strategies in this disease to improve clinical outcomes.

RESULTS
Study design and approach overview
To investigate whether the microbiota influences skin inflammatory immune responses and clinical outcomes in patients infected with *L. braziliensis*, we carried out an integrative analysis of a multiomics dataset. Samples collected from a cohort of 62 patients infected with *L. braziliensis* were used to generate the following datasets: (i) a total transcriptome RNA-seq dataset from 51 lesion biopsies collected before Sb^v treatment; (ii) a 16S-seq dataset of swabs collected from the surface of the lesion before Sb^v treatment and on follow-up visits for a subset of patients (visit days, 30 to 240); (iii) a library of *S. aureus* isolates cultured from the lesions and their genome sequences; and (iv) clinical metadata with patient demographics. The cohort consisted of 20 females and 42 males, with an average age of 30 years (range, 17 to 56 years). Clinical metadata collected included lesion size and location, delayed-type hypersensitive (DTH) measurements, lymphadenopathy, time to heal, and treatment outcome. In most cases, multiple sample types were collected from the same patient. The study design and inventory are detailed in fig. S1 and tables S1 and S2.

The lesional bacterial burden is associated with enhanced host inflammatory gene expression
To investigate the role of the skin microbiome in mediating host transcriptional pathways in *L. braziliensis* infections, we extracted RNA and made cDNA libraries from biopsies of leishmanial lesions and control skin of uninfected individuals. In parallel, with RNA-seq analysis, we used the same cDNA libraries to estimate lesional bacterial burden by quantitative polymerase chain reaction (qPCR) targeting of the prokaryotic 16S rRNA gene (Fig. 1A) and found that the bacterial burden was elevated in lesions compared with contralateral healthy skin, $P < 0.01$ (Fig. 1B). We performed a continuous differential gene expression (DGE) analysis and identified 148 host genes that positively correlated with the lesional bacterial burden (linear model slope coefficient > 0.2 and $P < 0.01$) (table S3). Gene Ontology (GO) analysis of this gene list revealed enrichment for proinflammatory immune responses, with a notable participation of genes encoding for members of the IL-1 signaling pathway (*IL1A*, *IL1B*, *IL1RN*, and *IL1R2*) and neutrophil chemotaxis, represented mainly by the CXCL family of chemotactic encoding genes (Fig. 1, C and D, and table S4). The *L. braziliensis* loads quantified in the biopsies by qPCR did not correlate with total bacterial burden (Spearman rho = 0.002, $P = 0.99$).

Our results suggest that high bacterial burden in the lesions drives proinflammatory gene expression programs, so we hypothesized that it may contribute to poor clinical outcomes in patients with *L. braziliensis*. On the basis of bacterial 16S rRNA transcript abundance in healthy contralateral skin, we split the cutaneous leishmaniasis cohort into high- and low–bacterial burden groups ($n = 26$ and $n = 25$ patients, respectively) and compared healing times. Patients with a high bacterial burden exhibited a delayed

response to therapy ($P = 0.05$), with some lesions persisting >300 days (Fig. 1E). These findings motivated further investigation into the lesional microbiota and its potential impact on the immunopathology associated with cutaneous leishmaniasis.

Staphylococcus often dominates the community structure of the lesional microbiota
To identify the bacteria that might be involved with delayed lesion resolution, we profiled microbiota of swab specimens collected from lesions and contralateral skin of patients with *L. braziliensis* before the start of therapy using 16S-seq (Fig. 2A). We found that the skin microbiome was markedly affected by infection with *L. braziliensis* relative to contralateral skin, with bacterial alpha diversity significantly lower in lesions as measured by the Shannon diversity index (Fig. 2B). Microbial community structure was also affected by *L. braziliensis* infection relative to contralateral skin, as calculated by the Weighted UniFrac dissimilarity metrics, a statistical method for comparing the composition between communities (Fig. 2C). To identify bacterial taxa enriched in lesions at baseline (before treatment), we performed differential taxa abundance analysis between the lesion and contralateral skin swabs. The genus *Staphylococcus* was the most differentially abundant genus in lesions, followed by *Corynebacterium* and *Streptococcus* [thresholds of fold change > 2 and false discovery rates (FDRs) < 0.05] (Fig. 2D). We also captured a signature of microbial communities present in the contralateral uninfected skin of the patients and identified the top five differentially abundant genera as *Nesterenkonia*, *Cutibacterium*, *Kocuria*, *Micrococcus*, and *Brachybacterium* (Fig. 2D). These genera are from the families *Propionibacteriaceae*, *Micrococciaceae*, and *Dermabacteraceae* and are commonly found on human skin in varying abundances (*11*).

To further investigate lesional bacterial communities, we reduced the dimensionality of the 16S-seq dataset to obtain the 10 most abundant taxa. Unsupervised hierarchical clustering (HC) analysis based on the relative abundance of these taxa revealed eight distinct microbiome profiles or "clusters" (Fig. 2, E and F). The thresholds that defined these clusters were based on a consensus of relative abundance mean (RAmean) per sample (fig. S2A) and number of dominant taxa in the community (>80% of total dominance and >2 taxa, respectively). The largest cluster, microbiome cluster 6 (M6), included 16 patients with lesions presenting dominant colonization by *Staphylococcus* (95% RAmean). This was followed by clusters M7, with seven patients presenting unique colonization by *Arcanobacterium* (56% RAmean), *Streptococcus* (17% RAmean), *Corynebacterium* (11% RAmean), and *Staphylococcus* (11% RAmean); M5, with six patients presenting a *Corynebacterium*-dominant colonization (80% RAmean); M4, with four patients with a *Streptococcus*-dominant colonization (90% RAmean); M3, with three patients presenting a co-colonization by *Streptococcus* and *Staphylococcus* (40 and 60% RAmeans, respectively); and two patients with either *Lactobacillus*- or *Finegoldia*-dominant colonization (M1 88% and M2 85% RAmean, respectively) (Fig. 2, E and F). Seven patients exhibited a more diverse microbiome with evenly distributed taxa. Their lesional microbiome profiles more closely resembled the contralateral skin microbiome and were enriched for taxa such as *Cutibacterium* (13% RAmean), *Bacillus* (19% RAmean), and *Kocuria* (13% RAmean). This microbiome cluster of lesions, M0, had a heterogeneous skin-like microbiota compared with the other clusters (Fig. 2, E and F). Because host-level factors
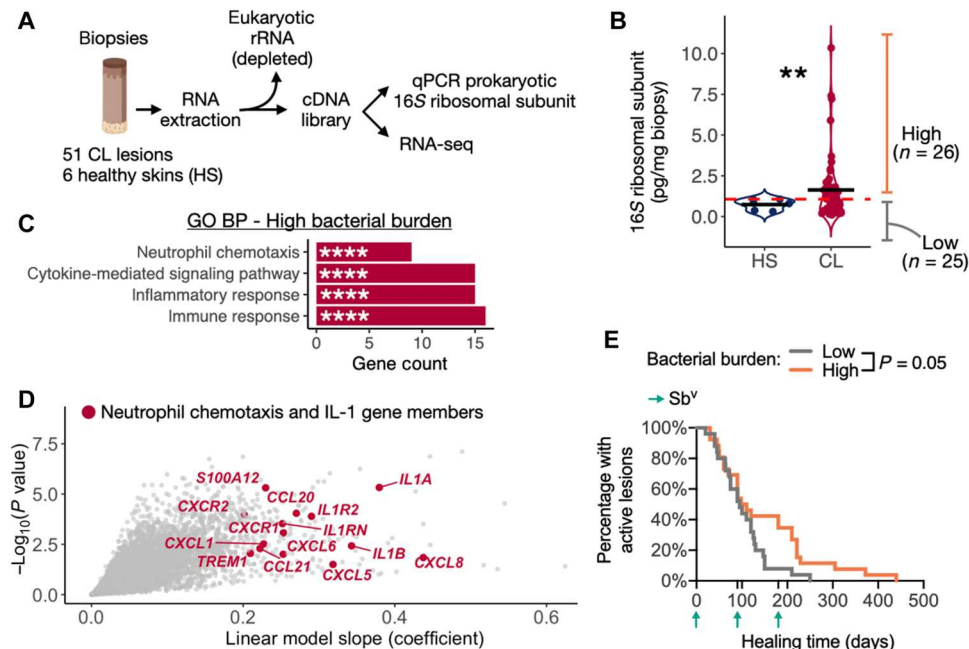
Fig. 1. Lesional bacterial burden is associated with enhanced proinflammatory gene expression and delayed healing time. (**A**) Schematics explaining the use of cDNA libraries from punch biopsies to perform RNA-seq and qPCR targeting the prokaryotic 16S rRNA gene to quantify total bacterial burden. Extracted RNA was depleted of eukaryotic rRNA before cDNA conversion. (**B**) Bacterial burden quantified by qPCR in biopsies collected from CL lesions and healthy skin (HS) control samples not infected by *L. braziliensis*. The mean for each group is represented, and a *t* test was used to calculate the statistical significance **$P < 0.01$. (**C**) GO BP analysis on the list of DEGs positively correlated with the continuous variable of bacterial burden (threshold of coefficient slope > 0.2 and $P < 0.01$). (**D**) DEGs highlight the genes annotated as Neutrophil chemotaxis and genes encoding for members of the IL-1 signaling. (**E**) Survival curve for lesion healing time comparing lesions with high and low bacterial burden. The threshold for dividing high and low bacterial burden lesions was based on the qPCR levels detected in HS biopsies. Log-rank (Mantel-Cox) test was used to calculate the statistical significance. GO BP, Gene Ontology with Biological Processes; ES, enrichment score; DEGs, differentially expressed genes.

can influence the skin microbiota, we used multivariate linear regression analysis to identify statistically significant associations between the microbiome clusters and clinical metadata. These analyses did not detect any statistically significant associations between these parameters (fig. S2B). However, we cannot rule out the size of the cohort as a limiting factor in detection. Together, these data show that infection by *L. braziliensis* drives the lesional microbiota to a variety of configurations in which *Staphylococcus* is the most frequent, consistent with our previous findings (*9*).

Stratification by microbiome profile reveals signatures associated with delayed clinical resolution

We next investigated whether lesional microbiome clusters were associated with delayed clinical resolution. We designated the M0 cluster as a reference control because of the heterogenous, skin-like microbiota characterizing these lesions. When we compared the healing times of clusters M1 to M7 with the M0 cluster, we observed a trend toward delayed clinical resolution, $P = 0.09$ (Fig. 3A, top). When we stratified the samples by microbiome cluster, M6 lesions were delayed in healing time compared with M0, $P = 0.02$ (Fig. 3A, bottom). The other microbiome clusters did not significantly differ in clinical outcome compared to M0. However, these clusters contained fewer samples, resulting in less statistical power (fig. S3A). Lesions from the M6 and M7 clusters presented increased *L. braziliensis* parasite burdens, measured by qPCR, compared with lesions in the M0 cluster (Fig. 3B). This is consistent with our

previous findings that increased parasite burdens are associated with treatment failure (*12*).

We considered the succession of lesional microbial communities over time and the relationship with clinical course. We calculated weighted UniFrac dissimilarity metrics on swab samples collected at the initial visit to the clinic (before treatment) and at follow-up visits (Fig. 3C and fig. S3B). Focusing this analysis on the M6 cluster, we compared patients who required >1 round of Sb^v treatment with those who were cured after a single treatment. In patients cured with one round of Sb^v, the lesional microbiome structure consistently shifted by day 60 to more closely resemble the contralateral skin community structure (Fig. 3C, left). Patients who required >1 round of Sb^v did not recover lesional signatures similar to skin communities by the end of follow-up (Fig. 3C, right). We also found that patients who required >1 round of Sb^v to heal exhibited individual marked microbiome structure shifts throughout the course of lesion development (Fig. 3C). A comparison of patients #54 and #55 provides an example of these dynamics. Patient #54, initially from the M6 cluster (*Staphylococcus* dominance), required two rounds of Sb^v treatment and did not heal until day 150. During this time, the lesional microbiome shifted to a *Streptococcus*-predominant colonization (similar to the M4 cluster profile) but, at the time of cure, returned to 80% *Staphylococcus* relative abundance (Fig. 3D). In contrast, patient #55 from the M0 cluster required only one round of Sb^v; was cured by day 60; and, at the time of cure, had a skin microbiome made up of taxa associated with a healthy microbiome, including *Cutibacterium*, *Bacillus*, and *Kocuria* (Fig. 3D). Weighted
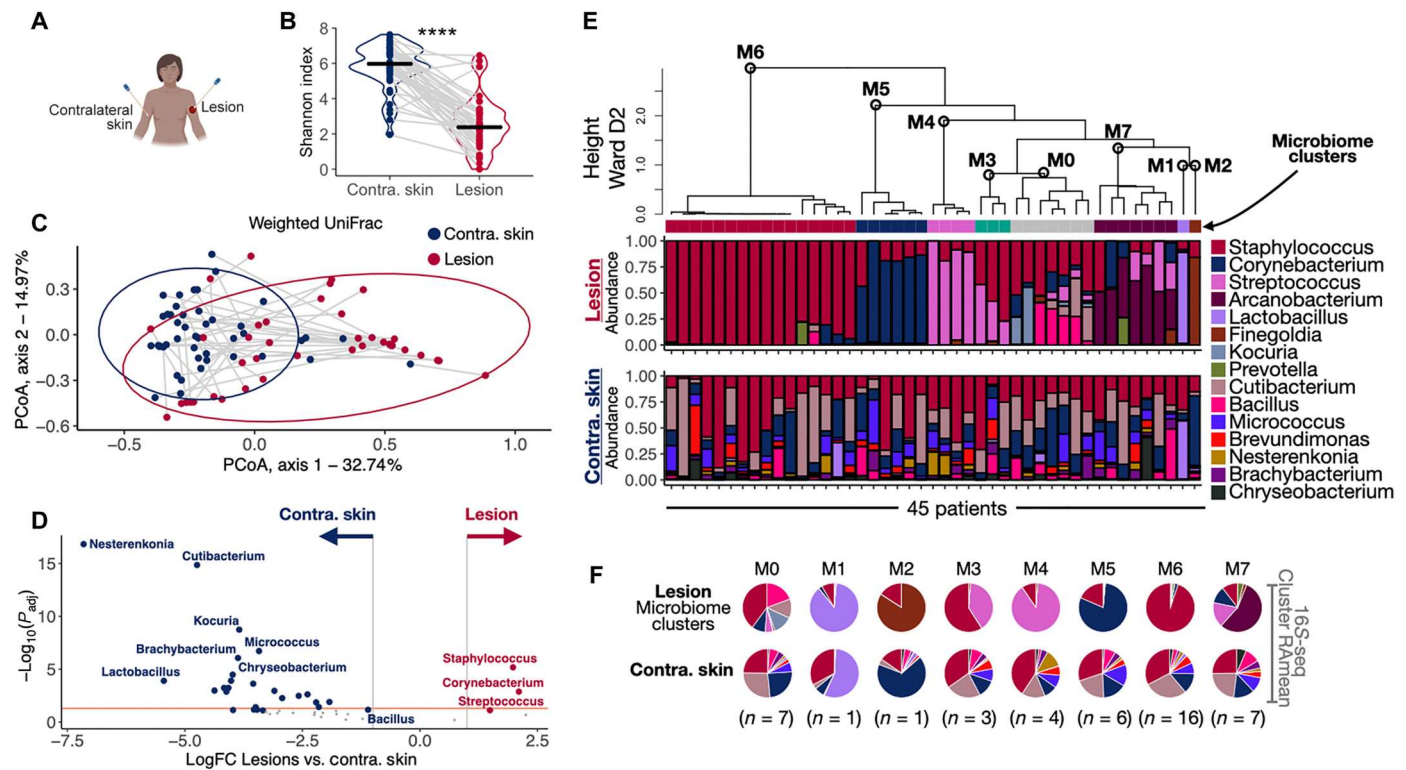
Fig. 2. *L. braziliensis*–infected lesions present distinct microbiome profiles. (**A**) Swabs were collected from the lesion and contralateral skin sites for 16*S*-seq analysis. (**B**) Shannon index assessed bacterial alpha diversity. Gray lines connect the lesion and contralateral skin samples collected from the same patient. Paired *t* test was used to calculate the statistical significance, ****$P < 0.0001$. (**C**) Principal coordinate analysis (PCoA) performed on the weighted UniFrac dissimilarity metrics (method to compare the composition between communities) showing lesion and contralateral skin microbiome profiles placed in coordinates 1 and 2. (**D**) Differential taxa abundance analysis between all the lesion and contralateral skin samples collected on day 0. The orange line indicates adjusted *P* value = 0.05. (**E**) Unsupervised HC calculated with Ward D2 agglomeration method clustered the lesion samples collected at day 0 by their top 10 genera microbiome profiles (clusters M0 to M7). The relative abundances of the top 10 taxa in the lesions are represented as stacked bar plots (top). The relative abundances associated with the microbiomes in the contralateral skin are represented right underneath the lesion sample from the same patient (bottom). (**F**) The RAmeans of each taxon in lesions and contralateral skin samples per microbiome cluster (M0 to M7) were calculated and visualized as a pie chart. FC, fold change.

UniFrac dissimilarity analysis calculated with the longitudinal data from the contralateral skin of M6 patients revealed that the antiparasitic Sb^v did not have a significant effect on the skin microbiome (fig. S3C). Thus, the longitudinal changes we observe in the lesional microbiome are unlikely driven by therapy alone.

Altered microbiomes are associated with enhanced proinflammatory lesional gene expression

We hypothesized that different configurations of the lesional microbiome would drive distinct inflammatory and immune responses. To test this, we performed a combination of principal components analysis (PCA) (fig. S4, A and B) and DGE analysis (table S5) to examine the relationship between microbiome clusters and lesional gene expression (Fig. 4). We first compared M4, M5, M6, and M7 clusters with the M0 reference cluster to identify differentially expressed genes (DEGs) (separate analysis), combined the DEGs results, and performed HC to identify gene modules. DGE analyses were not performed with lesions from M1 to M3 clusters because of small sample sizes in these clusters; however, they were included for unsupervised HC classification. The structure of the dendrogram suggested two major gene modules: module 1 with genes overexpressed in the M0 cluster and module 2 with genes overexpressed

in the M4 to M7 clusters. GO analysis revealed that module 1 was significantly enriched for cell adhesion, Wnt signaling, and nervous system development gene signatures (Fig. 4B, top, and table S6), suggesting the induction of wound healing and skin repair processes. Module 2 was significantly enriched for innate proinflammatory signatures, such as granulocyte/myeloid/lymphocyte-associated chemotaxis, response to cytokines such as interferon-γ, response to lipopolysaccharide, and apoptotic processes (Fig. 4B, bottom, and table S7). Examining the top 10 DEGs revealed that proinflammatory-related genes, including *IL1A* and *IL1B*, were overrepresented in the lesional transcriptional profiles of M1 to M7 compared with M0 lesions (Fig. 4C). These findings suggest that deviations in the lesional microbiome away from the skin-like M0 profile are associated with enhanced proinflammatory gene expression.

The magnitude of host proinflammatory responses correlates to the type of lesional microbiota

Because we observed a proinflammatory gene expression signature across all distinct microbiome clusters, we asked whether the magnitude and type of proinflammatory transcriptional programs might differ according to microbiome cluster. To test this, we used a previously described dataset-reductive computational
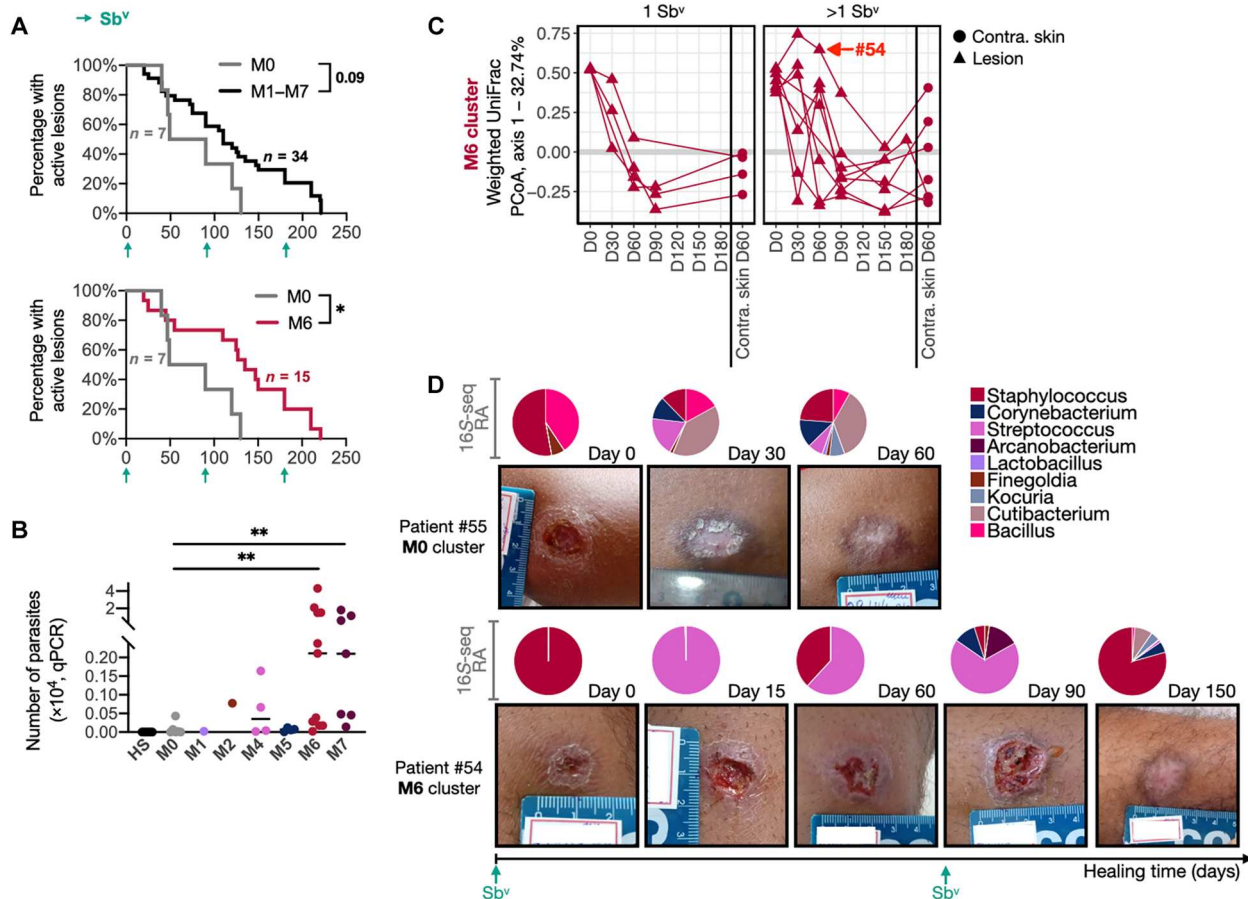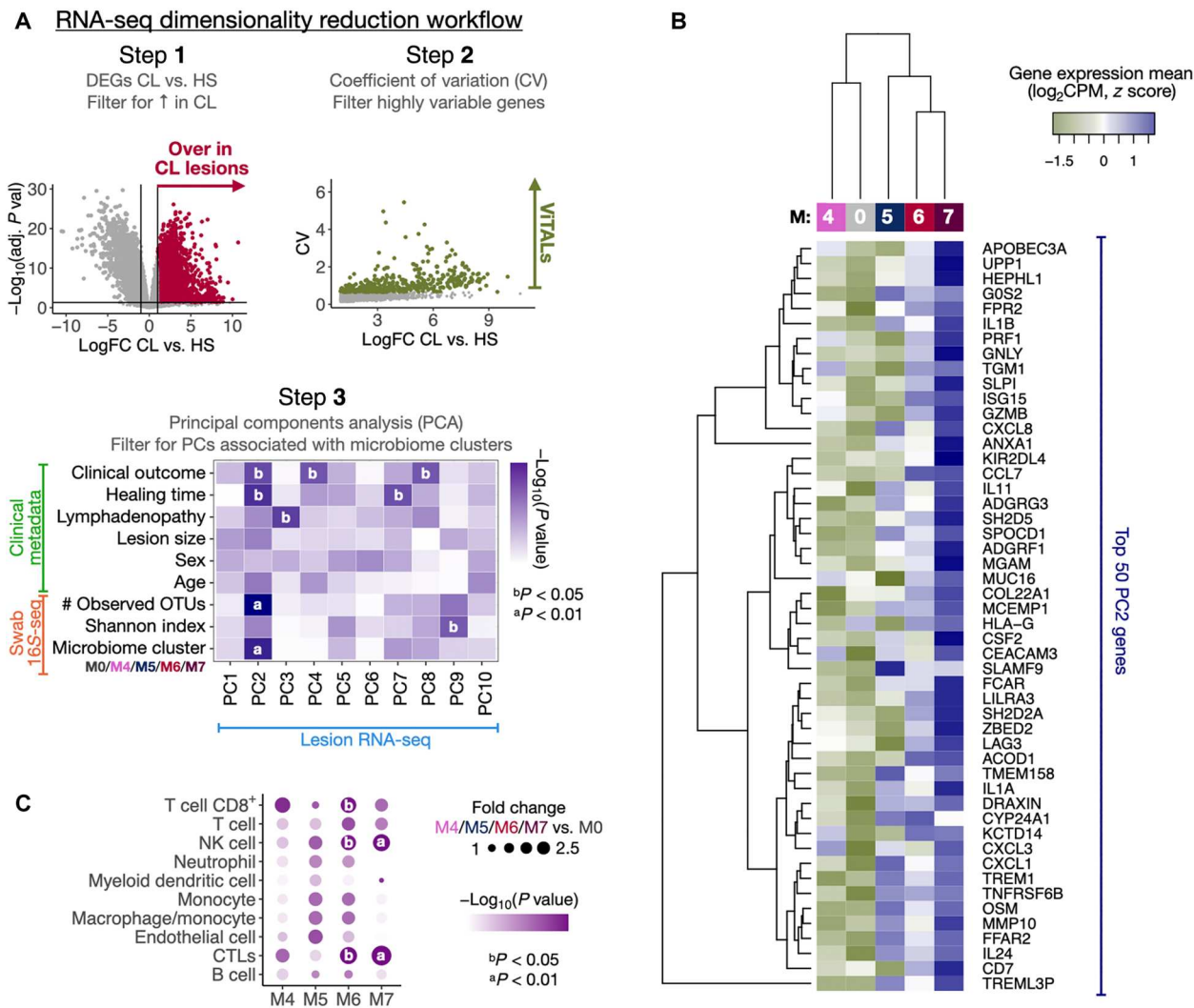
Fig. 3. Predominant colonization with *Staphylococcus* is associated with delayed healing time and disturbed microbiome recovery. (**A**) Survival curves for the healing time for lesions of patients from the M1 to M7 clusters combined versus M0 cluster and separately M6 versus M0 cluster. Patients who received an alternative form of treatment from an ongoing clinical trial in the clinic were not considered or added to the clinical outcome–related analysis. Log-rank (Mantel-Cox) test was used to calculate the statistical significance, *$P = 0.02$. (**B**) As measured by qPCR, the absolute number of parasites detected in 4-mm punch biopsies from CL lesions taken immediately before starting treatment. A *t* test was used for statistical testing, **$P < 0.01$. (**C**) PCoA showing component 1 calculated from weighted UniFrac dissimilarity analysis, including longitudinal swab samples from the M6 cluster (day 0 to day 180) and swab samples from the contralateral skin of the same patient. Patients were divided for analysis according to the number of Sb^v rounds required for complete healing (1 versus >1 round of Sb^v). The connecting lines indicate samples collected from the same patient over time. (**D**) Two representative examples of photographs taken from M0 (patient no. 55) and M6 (patient no. 54) lesion clusters. The relative abundance pie charts from 16*S*-seq profiling evaluated over time are indicated on top of the associated photos.

workflow (Fig. 5A) (*12*). Briefly, to enhance statistical power, we focused on genes whose expression was highly variable between the lesions and were therefore termed variable transcripts associated with lesions (ViTALs). We reduced the list of ViTALs to principal components (PCs) from PCA (Fig. 5A and table S8). These PCs were then associated with the 16*S*-seq and clinical metadata variables with multivariate linear regression analysis (Fig. 5A). PC2 had the strongest association with microbiome variables, including microbiome cluster and the number of observed operational taxonomic units (OTUs), a measure of alpha diversity (fig. S5A). PC2 was also associated with clinical outcomes (>1 round of Sb^v) and increased healing times [Fig. 5A, (step 3) bottom, and fig. S5, A and B]. Although PC1 accounted for a greater amount of variation in the dataset (26.01%, compared with 13.21% for PC2), it was not associated with clinical metadata or microbiome variables. We thus focused on defining the genes that were most strongly associated with PC2 (fig. S5B).

The top 50 genes associated with PC2 included genes encoding for cytotoxicity-associated effector molecules and receptors such as *PRF1*, *GNLY*, *GZMB*, and *KIR2DL4* (Fig. 5B). These genes, along with *APOBEC3A*, *ISG15*, and *LILRA3*, were previously identified as potential biomarkers for delayed treatment outcome (*12*). Other genes associated with PC2 encoded for neutrophil chemotaxis and effector functions, such as *CEACAM3*, *CXCL1* and *CXCL3*, and genes encoding for proinflammatory cytokines, such as IL-1α, IL-1β, oncostatin M (*OSM*), IL-24, and secretory leukocyte protease inhibitor (*SLPI*) (Fig. 5B). These top 50 PC2 genes were most highly expressed in lesions from microbiome clusters M6 and M7 and were least expressed in lesions from microbiome cluster M0. Although PC1 was not associated with clinical outcome or microbiome metrics, genes associated with PC1 included B cell response–related gene expression patterns (immunoglobulins and B cell receptor–encoding genes) (fig. S5B). Together, these findings support a relationship between the lesional microbiota, clinical
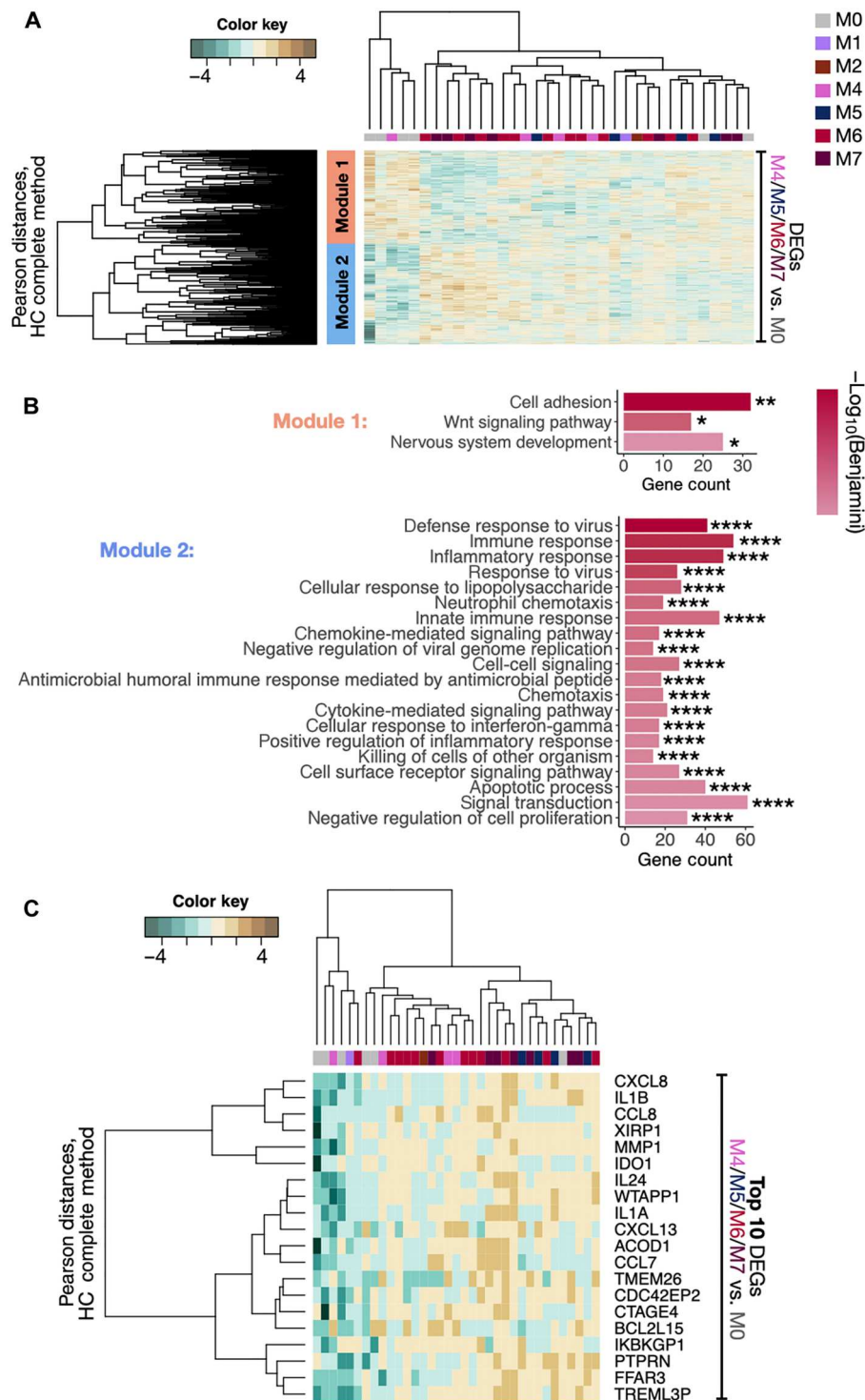
Fig. 4. An altered microbiome is associated with enhanced proinflammatory gene expression. (**A**) Separate DGE analyses were performed between lesions from the reference cluster M0 and clusters M4, M5, M6, and M7. The combined DEGs were then used to classify all lesions according to their transcriptional profiles by unsupervised HC ($P < 0.05$ and fold change > 1.5). DGE analyses were not performed with M1, M2, and M3 clusters because of insufficient sample size; however, they were included for unsupervised HC classification. Two gene modules were captured by Pearson's distances (module 1, orange; module 2, blue). (**B**) GO analysis for BP terms was carried out in the two gene modules from (A). Bar graphs represent the number of genes identified in the GO genesets, and the color scale represents the statistical strength calculated by Benjamini-Bonferroni multiple correction testing. *$P < 0.05$, **$P < 0.01$, ****$P < 0.0001$. (**C**) Top 10 genes from each DGE analysis performed between the lesions from clusters M4, M5, M6, and M7 compared with M0 were concatenated and used to classify all the CL lesions according to their transcriptional profiles by HC.

Farias Amorim *et al.*, *Sci. Transl. Med.* **15**, eadh1469 (2023)   18 October 2023

6 of 14

A RNA-seq dimensionality reduction workflow

Fig. 5. The distinct CL lesional microbiomes affect the proinflammatory gene expression profiles in different magnitudes. (**A**) A dataset dimensionality reduction computational workflow was performed to integrate output parameters from the three primary datasets included in this study (RNA-seq, 16S-seq, and clinical metadata). Briefly, the gene expression matrix from the RNA-seq was reduced to a list of ~400 genes overrepresented in CL versus HS (step 1), displaying high variability among CL samples as calculated by the coefficient of variation (CV) (step 2). Those genes were ViTALs and were further reduced to PCs in a PCA (step 3). A multivariate linear regression analysis was performed between the PCs and the 16S-seq parameters, and clinical metadata reduced output features. (**B**) Top 50 PC2-associated genes are displayed in a heatmap and classification of transcriptional profiles by the microbiome clusters M4 to M7 as calculated with HC. (**C**) MCP-counter was used to estimate the cell population abundances from the RNA-seq dataset. A differential cell population analysis was performed, and the results from M4, M5, M6, and M7 versus M0 are displayed as fold changes and P values.

outcome, and proinflammatory and cytotoxic transcriptional signatures but not with B cell–related responses.

Because we observed highly variable proinflammatory lesional expression profiles across the microbiome clusters, we reasoned that immune cell populations might similarly differ. We used the Microenvironment Cell Populations–counter (MCP-counter) method, which allows quantification of the absolute abundance of immune cells in bulk RNA-seq samples on a gene marker basis. We observed increased frequencies of myeloid, granulocyte, and lymphocyte cell populations in M4 to M7 versus M0 (fold change > 0). Cytotoxic T lymphocytes and natural killer (NK) cells were estimated to be significantly elevated in the lesions of M6 and M7 clusters compared with the M0 cluster ($P < 0.01$ for M7 and $P \leq$

0.05 for M6) (Fig. 5C). Furthermore, CD8+ T cells were estimated to be significantly increased in the M6 cluster ($P < 0.05$) (Fig. 5C). Together, these observations strongly suggest that lesions in the M6 and M7 microbiome clusters express clinical outcome–related proinflammatory transcriptional signatures.

S. aureus in lesion biopsies is associated with pathogenic inflammation and delayed healing time

We found that lesions falling into the M6 and M7 microbiome clusters were characterized by enhanced proinflammatory signatures and increased relative abundances of *Staphylococcus*. The genus *Staphylococcus* encompasses a range of species that differentially affect host immune responses. *S. epidermidis* is a critical skin

Farias Amorim *et al.*, *Sci. Transl. Med.* **15**, eadh1469 (2023)   18 October 2023

7 of 14

commensal in mammals that mediates protective and adaptive immune responses required for tissue homeostasis. In contrast, *S. aureus* is the most common cause of skin and soft tissue infections and comprises two-thirds of the *Staphylococcus* isolates cultured from lesions of patients in this cohort (Fig. 6A and table S8). However, resolving species and strains of *Staphylococcus* based on short amplicons of the 16*S* rRNA gene is challenging. Although swab specimens are attractive for the collection of lesional and wound microbiota because they are generally noninvasive, they may not reflect deeper tissue bacterial burden and/or viable and

replicating bacteria. Therefore, we focused our subsequent analysis on the pathogen *S. aureus*, with a refined RNA-seq pipeline to identify *S. aureus* transcripts in lesion biopsies.

We built a custom reference *S. aureus* pangenome derived from 13 *S. aureus* clinical isolates cultured from lesions in this cohort, improving our ability to detect *S. aureus* transcripts (fig. S6, A and B). These clinical isolates were all methicillin resistant. After whole-genome sequencing, the isolates were used to construct the *S. aureus* pangenome together with 22 publicly available genomes from *S. aureus* reference strains (Fig. 6, A and B, and fig. S6, A and
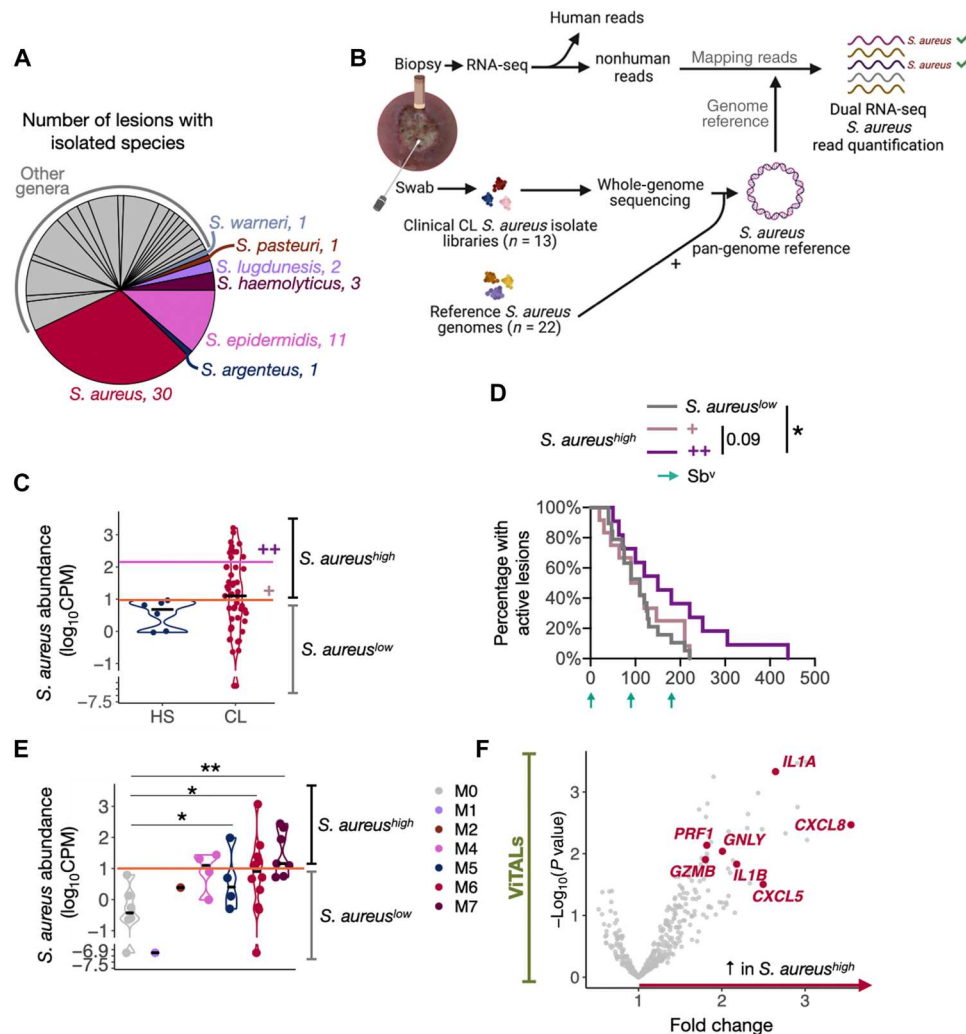
Fig. 6. Dual RNA-seq analysis with an in-house *S. aureus* pan-genome reference identified the potential host proinflammatory mechanisms associated with *S. aureus* abundances. (**A**) Name and number of clinical bacteria specimens isolated from 62 CL lesions. *Staphylococcus* spp. were annotated in the pie chart. (**B**) In-house *S. aureus* pangenome-based dual RNA-seq workflow to quantify and estimate *S. aureus* abundances in CL lesions. The nonhuman reads from the 51 CL RNA-seq samples were mapped to our pangenome reference, which is composed of genomes of 13 CL *S. aureus* clinical isolates and 22 *S. aureus* reference publicly available strains. (**C**) Abundance levels quantified in the six healthy RNA-seq lesion samples served as threshold ($\log_{10}$CPM = 1) to divide CL lesions into the groups of increased *S. aureus* abundances: *S. aureus*high lesions versus *S. aureus*low lesions. Twelve lesions presented overly high *S. aureus* abundances (*S. aureus*++, fold change = 18×) compared with 15 lesions with intermediate levels (*S. aureus*+, threshold = 2 $\log_{10}$CPM). (**D**) Survival curves for the healing time for *S. aureus*low lesions and *S. aureus*++ and + abundances (*S. aureus*high lesions). Patients who received an alternative form of treatment from an ongoing clinical trial in the clinic were not considered or added to the clinical outcome–related analysis. Log-rank (Mantel-Cox) test was used to calculate the statistical significance, *$P < 0.05$. (**E**) Abundance levels quantified in the CL RNA-seq lesion samples according to their corresponding 16*S*-seq microbiome cluster classification. The pink horizontal line indicates the threshold based on HS samples ($\log_{10}$CPM = 1). A *t* test was used to calculate the statistical significance, *$P < 0.05$ and **$P < 0.01$. (**F**) DGE analysis was performed with ViTALs between *S. aureus*high lesions and *S. aureus*low lesions (fold change > 1.5 and $P < 0.05$).
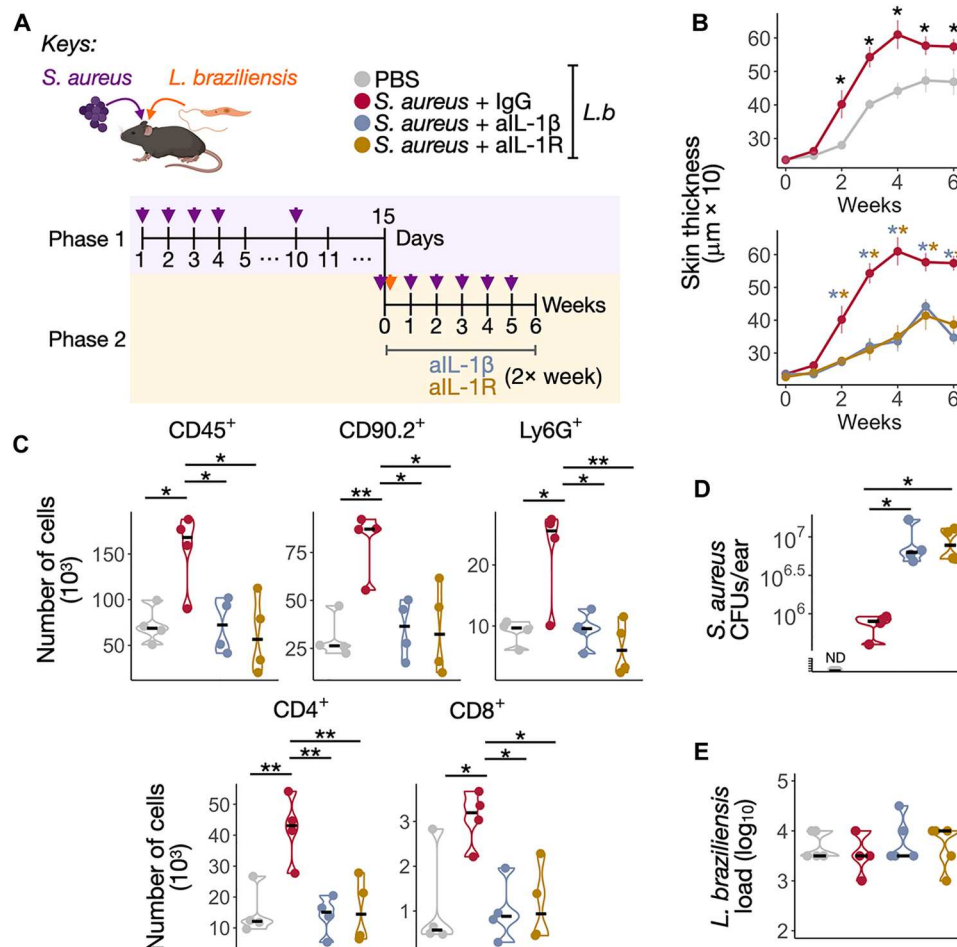
Fig. 7. _S. aureus_ and _L. braziliensis_ coinfection increases the inflammatory responses in an IL-1–dependent manner. (**A**) Schematic representation of _S. aureus_ and _L. braziliensis_ (_L.b_) treatment protocol in C57BL/6 mice divided in phase 1: pre–_S. aureus_ colonization and phase 2: _L. braziliensis_ infection course and blockade of IL-1β and IL-1R with monoclonal antibodies. Isotype IgG was used as a controlled treatment. The data shown are from one representative of two experiments (four to five animals per group). (**B**) Ear thickness measurements over time in mice. (**C**) Number of CD45^{+}, CD90.2^{+}, Ly6G^{+}, CD4^{+}, and CD8^{+} cells recovered from the coinfected ears. (**D**) Recovered pink _S. aureus_ colony-forming units (CFUs) and (**E**) parasite loads in the ear of different treatment groups in week six. Nonparametric Mann-Whitney test was used for statistical significance, *$P < 0.05$, **$P < 0.01$. Violin plots and median are represented in the plots. ND, not determined.

B). Transcripts that failed to map to the human reference were then mapped to the _S. aureus_ pangenome and quantified to estimate tissue burden. Relative to biopsies from uninfected, healthy skin, _S. aureus_ transcripts were elevated in 27 lesions (_S. aureus_[high]) (Fig. 6C and fig. S6C). Moreover, 12 of those lesions expressed overly high _S. aureus_ transcript abundances, around an 18-fold change, compared with lesions with intermediate levels (_S. aureus_ ++) (Fig. 6C and fig. S6C). We found that those _S. aureus_ ++ lesions were delayed in healing when compared with lesions with abundances similar to intact skin ($P < 0.05$) (Fig. 6D). Although the skin swabs did not show a dominance of _Staphylococcus_ in the M7 cluster, _S. aureus_ transcript abundances were increased in clinical isolates from these patients, suggesting that these bacteria may reside in deeper tissue not accessible by swabbing (Fig. 6E). Together, these findings indicate that the detection of _S. aureus_ transcripts in lesional tissue is indicative of a poor clinical outcome.

We investigated the lesion's host gene expression profiles that associated with transcriptionally active _S. aureus_ in the lesion. We performed a DGE analysis on the previously curated list of ViTALS to compare _S. aureus_[high] versus _S. aureus_[low] lesions (Fig. 6F and table S9). Genes enriched in _S. aureus_[high] lesions included _IL1A_, _IL1B_, _CXCL5_, _CXCL8_, _GNLY_, _PRF1_, and _GZMB_, all of which we previously associated with more severe disease in mice and treatment failure in patients (_12_). Furthermore, these genes were similarly up-regulated in lesions of the M7 and the M6 microbiome clusters, which were also characterized by high levels of _S. aureus_ transcripts. These findings provide strong evidence for potential immune mechanisms in which _S. aureus_ contributes to inflammation and clinical outcomes in leishmanial lesions.

S. aureus mediates IL-1–dependent pathology in a murine model of _L. braziliensis_ infection

On the basis of our findings in human lesions, we hypothesized that _S. aureus_ potentiates _Leishmania_ infection–induced proinflammatory programs that can influence disease outcomes. To directly test this, we colonized B6 mice with _S. aureus_ taken from a patient with _L. braziliensis_ (fig. S6B). Mice were colonized with bacteria and then infected with _L. braziliensis_ parasites (Fig. 7A). _S. aureus_

Farias Amorim _et al._, _Sci. Transl. Med._ **15**, eadh1469 (2023)   18 October 2023

9 of 14

colonization led to an increase in skin thickness when compared with control mice (Fig. 7B). Correspondingly, we found that lesions from *S. aureus*–colonized mice exhibited an increase in immune cells, particularly T cells (CD4⁺ and CD8⁺ cells) and neutrophils (Fig. 7C and fig. S7). These results indicate that *S. aureus* colonization promotes increased disease in mice by promoting an excessive inflammatory response. Because we found that human lesion biopsies with increased levels of *S. aureus* had enhanced transcription of the genes encoding IL-1 family members, we next blocked IL-1β or IL-1 receptor to test whether either was required for the increased pathology observed in mice. We found that neutralizing IL-1β or IL-1R significantly reduced the severity of the disease (Fig. 7, B and C). Whereas the depletion of IL-1 signaling lessened pathology, there was a concomitant increase in the *S. aureus* burdens (Fig. 7D). This result indicates that the pathology was immune-mediated rather than a direct effect of the bacteria. There was no significant change in the parasite burden in mice treated with anti–IL-1β or anti–IL-1R antibody (Fig. 7E). Together, these results implicate IL-1 as a critical factor driving increased disease severity in *S. aureus*–dominated lesions in mice and suggest that IL-1 can be a therapeutic target applicable to human cutaneous leishmaniasis.

DISCUSSION

L. braziliensis infections are associated with chronic ulcerative lesions and poor responses to drug treatment targeting the parasite (1–4, 13). Multiple factors could contribute to treatment failure (13, 14), one of which is the up-regulation of a cytolytic pathway mediated by CD8⁺ T cells and NK cells leading to inflammasome activation and IL-1β production (12). Here, we show that alterations in the skin microbiome also influence treatment outcomes. We analyzed a multiomics dataset that included 62 patients infected with *L. braziliensis* to profile and associate the skin microbiome with host gene expression and clinical metadata. We found that most patients infected with *L. braziliensis* exhibited an altered skin microbiome in their lesions most often dominated with *Staphylococcus*, whereas in a smaller number of patients, *Corynebacterium*, *Streptococcus*, or *Arcanobacterium* was dominant. Both the burden and the bacterial community structure influenced healing times, with *S. aureus* being an important species associated with delayed clinical outcomes. We also found that patients with higher levels of *S. aureus* exhibited increased expression of proinflammatory genes, including IL-1α and IL-1β. Last, neutralizing IL-1β signaling in mice colonized with *S. aureus* resulted in reduced IL-1–dependent pathology after *L. braziliensis* infection. Together, these results suggest that the skin microbiome in leishmanial lesions influences the progression of the disease and may delay healing time because of increased levels of IL-1.

To evaluate the association between the skin microbiome and clinical outcome in cutaneous leishmaniasis patients, we profiled the microbial composition of lesions and unaffected skin (contralateral skin from the same patient) by 16S-seq analysis. Most (84%) of the patients in this cohort developed alterations in their lesional microbiome. However, a few patients (16%) maintained a more diverse bacterial community similar to unaffected skin, which allowed us to compare the host transcriptional responses in these individuals with those observed in the lesions with altered microbiomes. Lesions with a modified microbiome were associated with seven distinct community structures (M1 to M7), but the most common was characterized by predominant colonization with *Staphylococcus* (M6, which includes 36% of the patients in this cohort). *Staphylococcus* was the genus most successfully isolated from lesions, as assessed by the number of clinical specimens isolated and cultured from the lesions. This observation suggests that *Staphylococcus* is particularly efficient in establishing itself in the ulcer caused by *L. braziliensis*, as previously reported in a separate cohort of *L. braziliensis*–infected patients by us (9) and others (15–17).

We used several computational approaches to investigate the interactions between the microbiome and host transcriptional profiles in cutaneous leishmaniasis. One involved a series of filtering steps to reduce the dimensionality of our datasets (16S-seq, RNA-seq, and clinical metadata) to integrate their main aspects (microbiome clusters and clinical outcome) and associate them with host gene expression by multivariate linear regression analysis. We also performed dual–RNA-seq analysis using an in-house *S. aureus* pangenome reference to estimate bacteria transcriptional abundances in each lesion. With these computational approaches, we found that both *S. aureus* abundances and an alteration on the microbiome composition are observed in cutaneous leishmaniasis. In addition, we identified a statistically significant correlation between the quantitative (total bacterial burden and *S. aureus* levels) and qualitative (specific microbiome community structures) factors with an increase in several proinflammatory genes. We identified that high expression of IL-1β gene is associated with bacterial alterations in leishmanial lesions and a delay in response to therapy. Further, we demonstrated that IL-1β increased disease in mice infected with *S. aureus* and *L. braziliensis*. These findings indicate that *S. aureus* contributes to immunopathology in leishmaniasis in an IL-1–dependent manner. This role for IL-1 in promoting pathology is consistent with other studies in experimental murine leishmaniasis (18–24) and with our human studies where we found that *IL1B* levels (but not IL1A) in lesions from patients with *L. braziliensis* are predictive of treatment failure (12). We previously identified two pathways that lead to IL-1β–dependent pathology, one of which is dependent on blocking IL-10 and leads to decreased parasite numbers but increased IL-1β–dependent pathology (24). The other pathway is initiated by cytolytic T cells that promote cell death, leading to NLRP3 activation and subsequent release of IL-1β (22, 25). Here, we show that a dysregulated skin microbiome is an additional pathway leading to increased disease dependent on IL-1β.

Biopsies from patients with high levels of *S. aureus* had elevated expression of cytolytic genes, such as those encoding *PRF1*, *GZMB*, and *GNLY*. Because increased *S. aureus* was associated with delayed healing, it is expected that cytolytic genes were also up-regulated, because we previously found that their expression predicted treatment failure (12). Thus, although a cytolytic pathway in other contexts can promote the control of some types of bacteria (26), that did not seem to be the case in this cohort. Instead, the tissue damage mediated by cytolytic T cells may provide the environment for *S. aureus* to invade and replicate in this patient population. This would be consistent with the ability of *S. aureus* to colonize broken skin and soft tissue (27, 28). However, the enrichment of genes associated with both cytolysis and IL-1 in *S. aureus*–dominant lesions is a feature of *L. braziliensis*–infected patients compared with other skin diseases complicated by *S. aureus* colonization and infection. In a similar analysis of atopic dermatitis (AD) and psoriasis

Farias Amorim *et al.*, *Sci. Transl. Med.* **15**, eadh1469 (2023) 18 October 2023

10 of 14

skin, Fyhrquist *et al.* (*27*) found that AD skin exhibited high levels of *S. aureus*, accompanied by transcriptional activation of T helper 2 (T$_H$2)–associated inflammatory pathways. Because T$_H$2 gene expression was not evident in this study, it appears that *S. aureus* can be associated with different inflammatory responses, depending on the context. We observed up-regulation of the itaconate (Irg1)–encoding gene ACOD1 in patients with altered microbiomes. In other contexts, itaconate was reported to inhibit the inflammasome activation and downstream IL-1β release (*29*), but we did not observe lower expression of IL1B in samples with high levels of ACOD1. However, it has also been reported that *S. aureus* increases itaconate, which limits bacterial killing, indicating a possible role in the increased *Staphylococcus* burdens (*28*).

The blockade of IL-1β/IL-1R in the murine experiments did not affect the parasite burden, whereas lesions from some patients with a dominant *Staphylococcus* microbiome (M6) showed increased *L. braziliensis* burdens. The potentially complex ecological and biological relationship between the parasite and specifically *S. aureus* has not been studied in patients, and host genetics, immune responses, and bacterial strains might all play a role in the increase in parasites in patients (and vice versa), which might not be replicated in inbred mice.

In addition to the *Staphylococcus*-dominated profiles, less frequently observed configurations of the microbiota were also observed in some patients. For example, one microbiome cluster was characterized by *Arcanobacterium* genera (M7 cluster), and we successfully cultured and isolated *Arcanobacterium haemolyticum* from leishmanial lesions (table S5). Lesions from those patients exhibited aberrant proinflammatory gene expression relative to the whole cohort of biopsy samples, including cytolysis-related genes and IL-1α/β–encoding genes. In addition, those lesions presented the highest abundance of *S. aureus* and parasites. *A. haemolyticum* is found in chronic wounds such as diabetic foot ulcers (*30*), as well as in soft-tissue infections from immunocompromised populations (carcinomas and other malignant tumors, rheumatism, hypertension, and gout) (*30*) together with *S. aureus*, *Corynebacterium diphtheriae*, and group A, C, or G *b-haemolytic streptococci* (*30, 31*). *A. haemolyticum* produces phospholipase D, which protects it from *S. aureus*–related hemolysis, and coinfection can lead to cellular necrosis in HeLa cells (*32*). Little is known about the impact of this specific microbiota configuration of the microbiota on the immune responses associated with other skin infections. Whereas the sample size of patients with *A. haemolyticum* was too low to associate with delayed healing, our results suggest that the *A. haemolyticum*–*S. aureus* community in leishmanial lesions may have a particularly detrimental impact on the clinical disease course. A limitation of this study is the relatively small sample sizes of patients whose lesional microbiomes were not predominantly dominated by *Staphylococcus*, which restricted our ability to provide a comprehensive assessment of host gene expression and clinical outcomes in these patients.

Cutaneous leishmaniasis is an infectious disease characterized by complex interactions between the host and the parasite. Here, we demonstrate that cutaneous leishmaniasis leads to marked changes in the skin microbiome. Using an integrative approach using clinical specimens and experimental murine infections, we directly demonstrate the microbiome's critical role in the outcome of leishmanial infection. With resistance to Sb^v increasing in many endemic areas, the search for alternative treatment strategies is crucial. Here, we provide additional evidence supporting immunotherapy targeting IL-1 to reduce the inflammatory responses seen in cutaneous leishmaniasis, such as anakinra or humanized anti–IL-1β canakinumab (*22*). Further, our results provide a rationale for new therapies to influence the skin microbiome in patients, which might be accomplished by antibiotics, probiotics, and improved strategies for care of the leishmanial lesion.

MATERIALS AND METHODS
Study design
Samples and metadata were collected from patients with *L. braziliensis* at a Leishmaniasis Reference Center in Corte de Pedra, Bahia, Brazil. The diagnosis of leishmaniasis was made by the documentation of DNA of *L. braziliensis* by PCR, isolation of parasites, or by a typical lesion and one of the following: DTH to leishmania antigen and histopathology. Exclusion criteria included previous anti-leishmanial treatment, individuals <18 years old, pregnancy, the presence of other comorbidities, or a positive serologic test for HIV. Informed consent was obtained from those enrolled in the study, after which lesions were measured and photographed. Lesions and contralateral skin were swabbed for 16*S*-seq microbiome profiling and to obtain bacterial isolates. Punch biopsies were collected from the border of the lesions and stored in RNAlater (Thermo Fisher Scientific, #AM7020). Additional biopsies from healthy controls were also collected. In most cases, different sample types were collected from the same patient. After collection of swabs and biopsies, patients were given standard-of-care treatment (daily intravenous injections of Sb^v; 20 mg/kg per day for 20 days). Patients were evaluated for lesion resolution on day 30 and every 30 days after treatment to assess healing. In a smaller cohort of patients, swabs for 16*S*-seq microbiome profiling and lesion photographs were collected at days 30 to 210 (fig. S1). This study was conducted according to the principles specified in the Declaration of Helsinki and under local ethical guidelines (Ethical Committee of the Faculdade de Medicina da Bahia, Universidade Federal da Bahia, Salvador, Bahia, Brazil, and the University of Pennsylvania Institutional Review Board #2.867.123).

Swab processing and microbiome profiling by 16*S*-seq
Swab specimens from lesions and contralateral skin were collected in sterile 0.15 M NaCl with 0.1% Tween 20 in 1× phosphate-buffered saline and stored at −20°C. Thirty-two negative control swab samples were exposed to air in the same room where the patients were seen and are called "environmental" samples. These samples were collected throughout patient recruitment and inclusion in this study. Genomic DNA extraction from swabs, library preparation, and 16*S*-seq from swab specimens were all performed at the Children's Hospital of Philadelphia (CHOP) High-throughput Sequencing and Analytical Core of the PennCHOP Microbiome Program. DNA was extracted using the QIACube HT robotic workstation for nucleic acid purification (Qiagen) together with the DNeasy 96 PowerSoil Pro QIAcube HT kit (Qiagen, #47021), per standard protocol. Amplification of the 16*S* rRNA gene V1 to V3 region was performed using primers forward 5′-AGAGTTTGAT CCTGGCTCAG-3′ and reverse 5′-ATTACCGCGGCTGCTGG-3′, followed by library preparation, quantification, and pooling, as previously described (*9*). Sequencing was performed on the Illumina MiSeq using 300-bp paired-end chemistry. Extraction blanks and

Farias Amorim *et al.*, *Sci. Transl. Med.* **15**, eadh1469 (2023) 18 October 2023

11 of 14

DNA-free water were subjected to the same amplification and purification procedure to assess potential environmental contamination. Samples with a total number of counts sequenced below the numbers detected in environmental control samples (<896 counts) were removed from further analysis accounting for 15 of 374 total samples, most of them from the contralateral skin of patients. The QIIME2 pipeline was used to process and analyze 16S-sequencing data using qiime2 q2cli version 2020.8.0. Briefly, samples were demultiplexed using demux and denoised using Dada2. Sequences were aligned using maaft, and phylogenetic trees were reconstructed using fasttree. Shannon Index alpha diversity metric was estimated using alpha-group-significance. Weighted UniFrac and Bray-Curtis beta diversity metrics were estimated using core-metrics-phylogenetic after samples were rarefied to 896 reads per sample, and P values were adjusted for multiple hypothesis testing using Benjamini-Hochberg FDR corrections. Taxonomy was assigned to sequences using q2-feature-classifier classify-sklearn against the Silva rRNA reference database, version 138 (silva-138-99-nb-classifier.qza). Taxa were collapsed to the genus. OTUs not present in at least 5% of the entire dataset were filtered out. The microbiome clustering classification was performed in the top 10 taxa versus lesion samples matrix in an untargeted manner, with HC and the Ward D2 agglomeration method.

Biopsy processing and RNA-seq gene expression profiling

Skin biopsies from the border of the open ulcers of patients and healthy skin from noninfected volunteers were homogenized with an MP tissue homogenizer (MP Biomedicals), and RNA was extracted using the RNeasy Plus Mini Kit (Qiagen, #74034) according to the manufacturer's instructions and used to prepare cDNA sequence–ready libraries using the Illumina TruSeq Total Transcriptome kit with Ribo-Zero Gold for eukaryotic cytoplasmic and mitochondrial rRNA depletion (Illumina). Quality assessment and quantification of RNA preparations and libraries were performed using an Agilent 4200 TapeStation and Qubit 3, respectively. Samples were sequenced five times to enhance sequencing depth on an Illumina NextSeq 500 to produce 75-bp single-end reads with a total mean sequencing depth of 42 million reads per biopsy sample. Raw reads were mapped to the human reference transcriptome (Ensembl; *Homo sapiens* version 100) using Kallisto version 0.46.0, and MultiQC v.18 was used to check the quality of the alignment. All subsequent analyses were conducted using the statistical computing environment R version 4.1.0, RStudio version 1.4.1717, and Bioconductor version 3.13. Briefly, transcript quantification data were summarized to genes using the BiomaRt and tximport package and normalized using the trimmed mean of M values method in edgeR. Genes with <1 counts per million (CPM) in at least six samples (the size of the smallest group of replicates, healthy skin) were filtered out. Normalized filtered data were variance-stabilized using the voom function in limma, and DGE analysis was performed with linear modeling using limma after correcting for multiple testing using Benjamini-Hochberg FDR correction. DGE analyses were performed between microbiome clusters with >3 samples (M4 to M7 versus M0). GO analyses were carried out using DAVID Bioinformatics Resources (2021 Update) from National Institute of Allergy and Infectious Diseases/National Institutes of Health and biological process terms and occasionally the Reactome, Kyoto Encyclopedia of Genes and Genomes, and Biocarta Pathway Database, clustering genesets by

annotation similarity. MCP-counter (33) and immunedeconv (34) R packages were combined to estimate cell population abundances from the RNA-seq dataset. Survival curves with log-rank (Mantel-Cox) testing were performed in GraphPad Prism version 8.

Dimensional reduction workflow and integration of datasets

We reduced the dimensionality of three primary datasets included in the study, and the main output parameters were used for integrative multivariate linear regression analysis. The reductive workflows and output parameters are as follows: (i) The biopsy whole transcriptome RNA-seq of around 17,000 mapped human coding genes in a sample versus gene matrix was reduced to a 401-gene list of "variable transcripts associated with lesions" (ViTALs) among lesion samples. This pipeline is described in our previous report (12) and available for reproducibility in the dockerized code "capsule" archived on Code Ocean (https://doi.org/10.24433/CO.5903311.v1). (ii) The whole swab 16S-seq dataset from samples collected at day 0 initiated at around 30,000 OTU matrix of patient samples after QC preprocessing; after a low-abundance filtering step, was collapsed to 86 individual, top frequent genera; and reduced to top 10 abundant taxa in lesion samples and lastly to eight microbiome clusters output by unsupervised HC with the Ward D agglomeration method (M0 to M7). The number of observed OTUs and Shannon Indexes per swab sample was also included as microbiome parameters. (iii) The clinical metadata parameters are categorical (clinical outcome: 1 or >1 Sb[v] rounds, sex, and presence of lymphadenopathy) and continuous variables (healing time in days, lesion size in square millimeters, and age in number of years). These output parameters were integrated using the rexposome framework (35). The rexposome outputs were modeled for visualization in R programming language using tidyverse R packages.

S. aureus isolate library, pan-genome reference, and quantification of *S. aureus* abundance in skin biopsies

Bacterial isolates were collected with a swab and stored immediately in cryotubes with freezing media [autoclaved, filtered tryptic soy broth (TSB) dissolved in deionized water with 1% sterile Tween 80% and 15% glycerol] at −20°C. For bacterial identification, swabs were removed from TSB and streaked out onto blood agar plates [tryptone soy agar (TSA) with sheep blood plate] (Remel, R01201) overnight at 37°C. Morphologically unique colonies were subcultured onto blood agar plates, and individual bacterial species were identified using Matrix-assisted laser desorption/ionization-time of flight (Pennsylvania Animal Diagnostic Laboratory System, New Bolton Center). After identification, *S. aureus* isolates were short-read whole-genome–sequenced. *S. aureus* DNA was extracted and purified using the Quick-DNA Fungal/Bacterial Miniprep Kit (Zymo Research, #D6005) and short-read paired-end Illumina Hiseq 2500–sequenced by the PennCHOP Microbiome Core. The in-house *S. aureus* pan-genome was built with the cutaneous leishmaniasis isolates and publicly available *S. aureus* reference genomes identifying the core and accessory genes with Roary (table S2) (36). *S. aureus* transcript identification and quantification were performed in the CL lesion RNA-seq files by mapping the reads post–filtering out human reads using KneadData to the *S. aureus* pan-genome. *S. aureus* abundances per RNA-seq lesion

sample represent the number of mapped counts per million (non-human) reads.

Quantification of bacterial burden in the skin biopsies by qPCR

The bacterial burden was quantified by qPCR from the same cDNA libraries used for lesional RNA-seq transcriptional profiling. A standard curve was prepared, followed by a cDNA library from *S. aureus* (subsp. *aureus* Rosenbach, 502A, American Type Culture Collection #27217). For this *S. aureus* standard curve, RNA was extracted by the RNeasy Plus Mini Kit (Qiagen, #74034), and cDNA conversion was prepared with the High-Capacity RNA-to-cDNA Kit (Applied Biosciences). qPCR was carried out on a ViiA 7 machine (Applied Biosciences) using Power SYBR Green Master Mix (Applied Biosciences) and primers targeting the 16*S* ribosomal subunit (357F_534R; forward 5′-CTCCTACGGGAGGCAGCAG-3′ and reverse 5′-AGAGTTTGATCCTGGCTCAG-3′) (*37, 38*). The qPCR results were normalized to the initial biopsy tissue weight. All reactions were carried out in duplicate, and data are represented as picogram per milligram of biopsy.

Quantification of parasite burden in the CL skin biopsies by qPCR

L. braziliensis burden in CL lesion biopsies was quantified as described previously (*12*).

S. aureus colonization and *L. braziliensis* infection

C57BL/6 mice (males, 6 to 8 weeks) were topically associated by applying up to 300 ml of suspended *S. aureus* (10^8 to 10^9 colony-forming units, CLSA50 from patient #50) to the ears and back of the mouse using sterile cotton swabs every day for a total of 4 days, once at day 10, once simultaneously with the *L. braziliensis* infection at day 15, and then once a week during the treatment protocol. On the basis of our published studies and preliminary data, we found that four or five mice per group allowed us to detect significant differences in lesion size. For infection, metacyclic promastigotes of *L. braziliensis* were isolated by Ficoll (Sigma-Aldrich) density gradient centrifugation and injected intradermally into the ear with 10^6 *L. braziliensis* parasites. Some mice were injected with 500 μg of anti–IL-β antibody, anti–IL-1R, or isotype immunoglobulin G (IgG) antibody (BioXcell, #BE0246, #BE0256, and #BE0297) twice a week for the duration of the experiment. Lesions were monitored by ear thickness. Parasite counts were performed by a limiting dilution assay. All experiments were approved by the institutional animal care and use committee at University of Pennsylvania (#804512).

Tissue processing and flow cytometry analysis

To prepare single-cell suspensions, ventral and dorsal sheets of the ears were separated from the cartilage and incubated for 90 min in a CO_2 incubator at 37°C in a 1-ml volume of RPMI 1640 (Sigma-Aldrich, #R7388) containing Liberase TL (0.25 mg ml^{-1}; Roche Diagnostics, #5401020001). The digested ears were passed through a 3-ml syringe to make single-cell suspension. The cells were filtered through a 70-μm nylon mesh and washed in fluorescence-activated cell sorting (FACS) buffer at 1500 rpm for 5 min. Cells were suspended in FACS buffer for further analysis. For surface staining, the following antibodies were used at 1:100 dilutions in FACS buffer according to the manufacturer's specifications: CD45 (30-F11, eBiosciences), CD3 (17A2, eBiosciences), CD90.2 (53-2.1, eBiosciences), βTCR (H57-597, eBiosciences), CD4 (RM4-5, BioLegend), CD8 (YTS5167.7, eBiosciences), CD11b (M1/70, eBiosciences), Ly6G (1A8, eBiosciences), and Ly6C (AL-21, BD Pharmingen). For counting the cells, AccuCount Fluorecent particles (Spherotech) were used. The stained cells were run on BD FACSymphony A3 (BD Biosciences), and the acquired data were analyzed using FlowJo software (Tree Star).

Supplementary Materials

This PDF file includes:
Figs. S1 to S7

Other Supplementary Material for this manuscript includes the following:
Tables S1 to S9
MDAR Reproducibility Checklist

REFERENCES AND NOTES

1. P. Kaye, P. Scott, Leishmaniasis: Complexity at the host-pathogen interface. *Nat. Rev. Microbiol.* **9**, 604–615 (2011).
2. P. Scott, F. O. Novais, Cutaneous leishmaniasis: Immune responses in protection and pathogenesis. *Nat. Rev. Immunol.* **16**, 581–592 (2016).
3. M. P. Oliveira-Neto, A. Schubach, M. Mattos, S. C. Goncalves-Costa, C. Pirmez, A low-dose antimony treatment in 159 patients with American cutaneous leishmaniasis: Extensive follow-up studies (up to 10 years). *Am. J. Trop. Med. Hyg.* **57**, 651–655 (1997).
4. A. Unger, S. O'Neal, P. R. L. Machado, L. H. Guimarães, D. J. Morgan, A. Schriefer, O. Bacellar, M. J. Glesby, E. M. Carvalho, Association of treatment of American cutaneous leishmaniasis prior to ulcer development with high rate of failure in northeastern Brazil. *Am. J. Trop. Med. Hyg.* **80**, 574–579 (2009).
5. T. A. Harris-Tryon, E. A. Grice, Microbiota and maintenance of skin barrier function. *Science* **376**, 940–945 (2022).
6. E. K. White, E. A. Grice, The wound microbiome. *Cold Spring Harb. Perspect. Biol.* **15**, a041218 (2023).
7. T. Y. Borbón, B. M. Scorza, G. M. Clay, F. L. N. de Queiroz, A. J. Sariol, J. L. Bowen, Y. Chen, B. Zhanbolat, C. P. Parlet, D. G. Valadares, S. L. Cassel, W. M. Nauseef, A. R. Horswill, F. S. Sutterwala, M. E. Wilson, Coinfection with leishmania major and Staphylococcus aureus enhances the pathologic responses to both microbes through a pathway involving IL-17A. *PLOS Neg. Trop. Dis.* **13**, e0007247 (2019).
8. S. Naik, N. Bouladoux, C. Wilhelm, M. J. Molloy, R. Salcedo, W. Kastenmuller, C. Deming, M. Quinones, L. Koo, S. Conlan, S. Spencer, J. A. Hall, A. Dzutsev, H. Kong, D. J. Campbell, G. Trinchieri, J. A. Segre, Y. Belkaid, Compartmentalized control of skin immunity by resident commensals. *Science* **337**, 1115–1119 (2012).
9. C. Gimblet, J. S. Meisel, M. A. Loesche, S. D. Cole, J. Horwinski, F. O. Novais, A. M. Misic, C. W. Bradley, D. P. Beiting, S. C. Rankin, L. P. Carvalho, E. M. Carvalho, P. Scott, E. A. Grice, Cutaneous leishmaniasis induces a transmissible dysbiotic skin microbiota that promotes skin inflammation. *Cell Host Microbe* **22**, 13–24.e4 (2017).
10. T. P. Singh, A. M. Carvalho, L. A. Sacramento, E. A. Grice, P. Scott, Microbiota instruct IL-17A-producing innate lymphoid cells to promote skin inflammation in cutaneous leishmaniasis. *PLOS Pathog.* **17**, e1009693 (2021).
11. E. A. Grice, J. A. Segre, The skin microbiome. *Nat. Rev. Microbiol.* **9**, 244–253 (2011).
12. C. F. Amorim, F. O. Novais, B. T. Nguyen, A. M. Misic, L. P. Carvalho, E. M. Carvalho, D. P. Beiting, P. Scott, Variable gene expression and parasite load predict treatment outcome in cutaneous leishmaniasis. *Sci. Transl. Med.* **11**, eaax4204 (2019).
13. A. Ponte-Sucre, F. Gamarro, J.-C. Dujardin, M. P. Barrett, R. López-Vélez, R. García-Hernández, A. W. Pountain, R. Mwenechanya, B. Papadopoulou, Drug resistance and treatment failure in leishmaniasis: A 21st century challenge. *PLOS Negl. Trop. Dis.* **11**, e0006052 (2017).
14. V. Mosimann, A. Neumayr, D. H. Paris, J. Blum, Liposomal amphotericin B treatment of Old World cutaneous and mucosal leishmaniasis: A literature review. *Acta Trop.* **182**, 246–250 (2018).
15. T. D. Jayasena Kaluarachchi, P. M. Campbell, R. Wickremasinghe, S. Ranasinghe, R. Wickremasinghe, S. Yasawardene, H. De Silva, C. Menike, M. C. K. Jayarathne, S. Jayathilake, A. Dilhari, A. J. McBain, M. M. Weerasekera, Distinct microbiome profiles and

biofilms in *Leishmania donovani*-driven cutaneous leishmaniasis wounds. *Sci. Rep.* **11**, 23181 (2021).

16. V. R. Salgado, A. T. L. de Queiroz, S. S. Sanabani, C. I. de Oliveira, E. M. Carvalho, J. M. L. Costa, M. Barral-Netto, A. Barral, The microbiological signature of human cutaneous leishmaniasis lesions exhibits restricted bacterial diversity compared to healthy skin. *Mem. Inst. Oswaldo Cruz* **111**, 241–251 (2016).

17. L. de Fátima Antonio, M. R. Lyra, M. N. Saheki, A. de Oliveira Schubach, L. de Freitas Campos Miranda, M. de Fatima Madeira, M. C. da Silva Lourenço, A. Fagundes, É. A. D. S. Ribeiro, L. Barreto, M. I. F. Pimentel, Effect of secondary infection on epithelialisation and total healing of cutaneous leishmaniasis lesions. *Mem. Inst. Oswaldo Cruz* **112**, 640–646 (2017).

18. S. L. Kostka, J. Knop, A. Konur, M. C. Udey, E. von Stebut, Distinct roles for IL-1 receptor type I signaling in early versus established leishmania major infections. *J. Invest. Dermatol.* **126**, 1582–1589 (2006).

19. J. E. Sims, D. E. Smith, The IL-1 family: Regulators of immunity. *Nat. Rev. Immunol.* **10**, 89–102 (2010).

20. K. Kautz-Neu, S. L. Kostka, S. Dinges, Y. Iwakura, M. C. Udey, E. von Stebut, A role for leukocyte-derived IL-1RA in DC homeostasis revealed by increased susceptibility of IL-1RA-deficient mice to cutaneous leishmaniasis. *J. Invest. Dermatol.* **131**, 1650–1659 (2011).

21. E. Voronov, S. Dotan, L. Gayvoronsky, R. M. White, I. Cohen, Y. Krelin, F. Benchetrit, M. Elkabets, J. Huszar, J. El-On, R. N. Apte, IL-1-induced inflammation promotes development of leishmaniasis in susceptible BALB/c mice. *Int. Immunol.* **22**, 245–257 (2010).

22. F. O. Novais, A. M. Carvalho, M. L. Clark, L. P. Carvalho, D. P. Beiting, I. E. Brodsky, E. M. Carvalho, P. Scott, CD8+ T cell cytotoxicity mediates pathology in the skin by inflammasome activation and IL-1β production. *PLOS Pathog.* **13**, e1006196 (2017).

23. D. Santos, T. M. Campos, M. Saldanha, S. C. Oliveira, M. Nascimento, D. S. Zamboni, P. R. Machado, S. Arruda, P. Scott, E. M. Carvalho, L. P. Carvalho, IL-1β production by intermediate monocytes is associated with immunopathology in cutaneous leishmaniasis. *J. Invest. Dermatol.* **138**, 1107–1115 (2018).

24. C. Gonzalez-Lombana, C. Gimblet, O. Bacellar, W. W. Oliveira, S. Passos, L. P. Carvalho, M. Goldschmidt, E. M. Carvalho, P. Scott, IL-17 mediates immunopathology in the absence of IL-10 following leishmania major infection. *PLOS Pathog.* **9**, e1003243 (2013).

25. F. O. Novais, L. P. Carvalho, J. W. Graff, D. P. Beiting, G. Ruthel, D. S. Roos, M. R. Betts, M. H. Goldschmidt, M. E. Wilson, C. I. de Oliveira, P. Scott, Cytotoxic T cells mediate pathology and metastasis in cutaneous leishmaniasis. *PLOS Pathog.* **9**, e1003504 (2013).

26. M. Walch, F. Dotiwala, S. Mulik, J. Thiery, T. Kirchhausen, C. Clayberger, A. M. Krensky, D. Martinvalet, J. Lieberman, Cytotoxic cells kill intracellular bacteria through granulysin-mediated delivery of granzymes. *Cell* **157**, 1309–1323 (2014).

27. N. Fyhrquist, G. Muirhead, S. Prast-Nielsen, M. Jeanmougin, P. Olah, T. Skoog, G. Jules-Clement, M. Feld, M. Barrientos-Somarribas, H. Sinkko, E. H. van den Bogaard, P. L. J. M. Zeeuwen, G. Rikken, J. Schalkwijk, H. Niehues, W. Däubener, S. K. Eller, H. Alexander, D. Pennino, S. Suomela, I. Tessas, E. Lybeck, A. M. Baran, H. Darban, R. S. Gangwar, U. Gerstel, K. Jahn, P. Karisola, L. Yan, B. Hansmann, S. Katayama, S. Meller, M. Bylesjö, P. Hupé, F. Levi-Schaffer, D. Greco, A. Ranki, J. M. Schröder, J. Barker, J. Kere, S. Tsoka, A. Lauerma, V. Soumelis, F. O. Nestle, B. Homey, B. Andersson, H. Alenius, Microbe-host interplay in atopic dermatitis and psoriasis. *Nat. Commun.* **10**, 4703 (2019).

28. K. L. Tomlinson, S. A. Riquelme, S. U. Baskota, M. Drikic, I. R. Monk, T. P. Stinear, I. A. Lewis, A. S. Prince, Staphylococcus aureus stimulates neutrophil itaconate production that suppresses the oxidative burst. *Cell Rep.* **42**, 112064 (2023).

29. A. Hooftman, S. Angiari, S. Hester, S. E. Corcoran, M. C. Runtsch, C. Ling, M. C. Ruzek, P. F. Slivka, A. F. McGettrick, K. Banahan, M. M. Hughes, A. D. Irvine, R. Fischer, L. A. J. O'Neill, The immunomodulatory metabolite itaconate modifies NLRP3 and inhibits inflammasome activation. *Cell Metab.* **32**, 468–478.e7 (2020).

30. T. Y. Tan, S. Y. Ng, H. Thomas, B. K. Chan, Arcanobacterium haemolyticum bacteraemia and soft-tissue infections: Case report and review of the literature. *J. Infect.* **53**, e69–e74 (2006).

31. H. Miyamoto, T. Suzuki, S. Murakami, M. Fukuoka, Y. Tanaka, T. Kondo, T. Nishimiya, K. Suemori, H. Tauchi, H. Osawa, Bacteriological characteristics of Arcanobacterium haemolyticum isolated from seven patients with skin and soft-tissue infections. *J. Med. Microbiol.* **64**, 369–374 (2015).

32. E. A. Lucas, S. J. Billington, P. Carlson, D. J. McGee, B. H. Jost, Phospholipase D promotes Arcanobacterium haemolyticum adhesion via lipid raft remodeling and host cell death following bacterial invasion. *BMC Microbiol.* **10**, 270 (2010).

33. E. Becht, N. A. Giraldo, L. Lacroix, B. Buttard, N. Elarouci, F. Petitprez, J. Selves, P. Laurent-Puig, C. Sautès-Fridman, W. H. Fridman, A. de Reyniès, Estimating the population abundance of tissue-infiltrating immune and stromal cell populations using gene expression. *Genome Biol.* **17**, 218 (2016).

34. G. Sturm, F. Finotello, F. Petitprez, J. D. Zhang, J. Baumbach, W. H. Fridman, M. List, T. Aneichyk, Comprehensive evaluation of transcriptome-based cell-type quantification methods for immuno-oncology. *Bioinformatics* **35**, i436–i445 (2019).

35. C. Hernandez-Ferrer, G. A. Wellenius, I. Tamayo, X. Basagaña, J. Sunyer, M. Vrijheid, J. R. Gonzalez, Comprehensive study of the exposome and omic data using rexposome bioconductor packages. *Bioinformatics* **35**, 5344–5345 (2019).

36. A. J. Page, C. A. Cummins, M. Hunt, V. K. Wong, S. Reuter, M. T. G. Holden, M. Fookes, D. Falush, J. A. Keane, J. Parkhill, Roary: Rapid large-scale prokaryote pan genome analysis. *Bioinformatics* **31**, 3691–3693 (2015).

37. K. Watanabe, Y. Kodama, S. Harayama, Design and evaluation of PCR primers to amplify bacterial 16S ribosomal DNA fragments used for community fingerprinting. *J. Microbiol. Methods* **44**, 253–262 (2001).

38. S. Turner, K. M. Pryer, V. P. Miao, J. D. Palmer, Investigating deep phylogenetic relationships among cyanobacteria and plastids by small subunit rRNA sequence analysis. *J. Eukaryot. Microbiol.* **46**, 327–338 (1999).

Farias Amorim *et al.*, *Sci. Transl. Med.* **15**, eadh1469 (2023)   18 October 2023

14 of 14

Science Translational Medicine

Multiomic profiling of cutaneous leishmaniasis infections reveals microbiota-driven mechanisms underlying disease severity

Camila Farias Amorim, Victoria M. Lovins, Tej Pratap Singh, Fernanda O. Novais, Jordan C. Harris, Alexsandro S. Lago, Lucas P. Carvalho, Edgar M. Carvalho, Daniel P. Beiting, Phillip Scott, and Elizabeth A. Grice

View the article online
https://www.science.org/doi/10.1126/scitranslmed.adh1469
Permissions
https://www.science.org/help/reprints-and-permissions

Use of this article is subject to the Terms of service